AGU PUBLICATIONS

JGR

Journal of Geophysical Research: Biogeosciences

RESEARCH ARTICLE

10.1002/2017JG004108

Key Points:
- Ecosystem productivity was more sensitive to hillslope convergence and divergence than spatial patterns of topoclimate
- Spatial patterns of ecosystem productivity become highly organized by topographic convergence as climatic water limitations intensify
- Hillslope convergence leads to enhanced and sustained photosynthetic activity across gradients in topoclimate

Supporting Information:
- Supporting Information S1
- Data Set S1
- Figure S1

Correspondence to:
Z. H. Hoylman,
zhoylman@gmail.com

Citation:
Hoylman, Z. H., Jencso, K. G., Hu, J., Martin, J. T., Holden, Z. A., Seielstad, C. A., & Rowell, E. M. (2018). Hillslope topography mediates spatial patterns of ecosystem sensitivity to climate. *Journal of Geophysical Research: Biogeosciences*, *123*, 353–371. https://doi.org/10.1002/2017JG004108

Received 7 AUG 2017
Accepted 11 JAN 2018
Accepted article online 15 JAN 2018
Published online 17 FEB 2018

Hillslope Topography Mediates Spatial Patterns of Ecosystem Sensitivity to Climate

Zachary H. Hoylman[1], Kelsey G. Jencso[1], Jia Hu[2], Justin T. Martin[2], Zachary A. Holden[3], Carl A. Seielstad[4], and Eric M. Rowell[4]

[1]Department of Forest Management, W.A. Franke College of Forestry and Conservation, University of Montana, Missoula, MT, USA, [2]Department of Ecology, Montana State University, Bozeman, MT, USA, [3]USDA Forest Service, Northern Region, Missoula, MT, USA, [4]National Center for Landscape Fire Analysis, W.A. Franke College of Forestry and Conservation, University of Montana, Missoula, MT, USA

Abstract Understanding how hillslope topography modulates ecosystem dynamics across topoclimatic gradients is critical for predicting future climate change impacts on vegetation function. We examined the influence of hillslope topography on ecosystem productivity, structure, and photosynthetic activity across a range of water and energy availability using three independent methods in a forested watershed (Montana, USA): 308 tree cores; light detection and ranging quantification of stem density, basal area, foliar biomass, and total biomass; and the enhanced vegetation index (EVI; 1984–2012). Multiple linear regression analysis across three conifer species revealed significant increases in measured basal area increment growth rates (from 56 to 2,058 mm^2/yr) with increasing values of the topographic wetness index and decreases in the climatic water deficit. At the watershed scale, we observed strong gradients in total biomass (e.g., 52 to 75 Mg/ha), which increased from ridgelines to convergent hollows. The most predominant topographic organization of forest biomass occurred along locations of climatically driven water limitations. Similarly, an analysis of growing season EVI indicated enhanced photosynthetic activity and a prolonged growing season in convergent hillslope positions. Collectively, these analyses confirm that within water-limited landscapes, meter-scale differences in topographic position can mediate the effects of the local energy balance and contribute to large differences in local hydrometeorological processes that are a necessary consideration for quantifying spatial patterns of ecosystem productivity. Further, they suggest that local topography and its topology with regional climate may become increasingly important for understanding spatial patterns of ecosystem productivity, mortality, and resilience as regional climates become more arid.

1. Introduction

The role of microclimates for mediating ecosystem processes in topographically complex regions has emerged as an important theme in the fields of ecology and hydrology (Dobrowski, 2011; Emanuel et al., 2011; McLaughlin et al., 2017; Running, 1984; Turner & Gardner, 2015). However, interactions between microclimate and broader scale orographic and regional patterns of energy and moisture remain poorly characterized. Improved understanding of the fine-scale ecosystem interactions with water and energy across topographic and climatic gradients is of paramount importance for forested mountainous environments (Rasmussen, 2012; Rasmussen et al., 2011), which are expected to experience the largest climate-induced changes (Barnett et al., 2005; Tague & Dugger, 2010). Changing water and energy availability will impact regional vegetation phenology (Richardson et al., 2013), ecosystem structure and function (Grimm et al., 2016), species mortality rates (McDowell & Allen, 2015), and zones of drought refugia (Dobrowski & Parks, 2016; McLaughlin et al., 2017).

In water limited montane environments, local hillslope topography may mediate environmental limitations on forest growth, contributing to fine spatial variability in rates of annual net productivity, forest structure, ecosystem response to seasonal drought, and longer term climatic change. Although gradients in climate due to orography and radiative forcing are commonly accepted as first-order drivers of vegetation productivity (Bonan, 2015), holistic conceptual models that incorporate the role of topographically induced microclimate, soil water, and shallow subsurface flow in complex terrain have not been developed. Here we demonstrate that local hillslope topographic convergence and divergence directly impacts the sensitivity of ecosystem productivity to regional climate signals across a range of conifer species and climatically driven water deficits.

Ecosystem productivity is highly impacted by water and energy availability (Biederman et al., 2016; Churkina & Running, 1998; Martin et al., 2017; Rosenzweig, 1968) due to the links between transpiration, photosynthesis, and carbon sequestration at the plant level. Water movement from soil reservoirs to foliage is facilitated by water potential gradients in root, xylem, and leaf tissues (Kramer & Boyer, 1995). Transpiration increases negative water potentials at the leaf surface, promoting water movement from the soil to replenish moisture lost to transpiration (Kramer & Boyer, 1995). Generally, as water limitations in the soil arise, conifer transpiration (and therefore photosynthesis and cellular division) is reduced as stomata close, thereby deterring extreme water potential gradients in plant tissue (Franks et al., 2007). However, the spatial locations and temporal durations of water limitation in mountain terrain can be highly variable due to topography.

Forests are generally considered to be net terrestrial carbon sinks (Pan et al., 2011), where a large portion of that sink is constrained to the woody biomass of northern forests (Myneni et al., 2001). Regional-scale distributions of water and energy interact in space and time to promote or restrict terrestrial ecosystem productivity, and therefore the carbon balance. Additionally, forest carbon uptake is widely considered to vary along elevation gradients (Bonan, 2015) as orographic processes drive precipitation distributions and available thermal energy. Radiant and thermal energy (hence forth "energy") distributions are known to impact physiological processes in conifers (Rossi et al., 2008; Vapaavuori et al., 1992) such as the timing of bud break and the onset of growth after winter dormancy (Hänninen & Tanino, 2011; Körner, 2006; Rossi et al., 2011), which partially dictate the duration of the conifer growing season by means of growth onset. Optimal growing conditions generally occur where warmer temperatures and increased water availability align, typically in middle elevations (Gholz, 1982; Rosenzweig, 1968; Whittaker & Niering, 1975).

Across mountain landscapes, hydrologic and near-surface atmospheric fluxes can vary spatially due to the complexity of the landscape. Topographic convergence and divergence (i.e., zero-order hillslope valleys versus ridgelines) have been well established as a first-order control on the organization and redistribution of water and energy fluxes (Hock & Holmgren, 2005; Jencso et al., 2009; Western et al., 1999; Western & Grayson, 1998). Some example processes that have been correlated with convergent hillslope positions include enhanced soil moisture due to wind redistribution of snowpack during the winter (Winstral & Marks, 2002), evaporative differences due to reductions in solar radiation (Fu & Rich, 2002; Tovar-Pescador et al., 2006), microclimate and cold air drainage that reduce vapor pressure deficits and evaporative demand (Chen et al., 1999; Novick et al., 2016), the accumulation of fine soil particles that lead to enhanced water holding capacity (Pachepsky et al., 2001), increased persistence of shallow soil moisture (Western & Greyson, 1998; Western et al., 1999), and the propensity for initiation of lateral subsurface flow that may subsidize vegetation along hydrologically connected downslope flowpaths (Hwang et al., 2012; Jencso & McGlynn, 2011).

A common theme that arises among an array of documented hydrometeorological and morphological processes is that topographic convergence generally leads to wetter conditions in both the shallow subsurface and atmosphere. However, some of these processes may contribute to the coevolution of plant available water and productivity while others may not. This is likely dependent upon the location and topology of local hillslope topography within regional and topoclimate (orography and radiation) gradients and local soil properties. Previous studies seeking to link hydrometeorological processes to plant growth have identified various topographic factors, which influence conifer stemwood productivity. Some examples include slope aspect (Fekedulegn et al., 2003; Oberhuber & Kofler, 2000), slope magnitude (Oberhuber & Kofler, 2000), elevation (Barnard et al., 2017), and landscape position (Adams et al., 2014). Additionally, topographic features such as upslope area, slope, and curvature have been observed as predictors of relative vegetation greenness (Flores Cervantes et al., 2014) and forest carbon accumulation (Swetnam et al., 2017). These studies, among others, have identified aspects of topography that impact spatial patterns of ecosystems at the watershed scale. However, few studies have combined independent ecological data sets from the plot to watershed scales, a requisite for advancing our understanding of the driving ecohydrologic processes that contribute to these spatial patterns. Furthermore, describing the sensitivity of ecosystems to topographically induced microclimate as a function of climatically driven soil water availability provides insight to how ecosystem patterns may respond to climate change (Allen et al., 2010; IPCC, 2014).

Here we use multiple independent data sets to examine the role of hillslope topography in organizing spatial and temporal patterns of ecosystem productivity and biomass across orographic and radiative gradients of water and energy availability at the Lubrecht Experimental Forest, western Montana. We quantified stem basal area growth rates, watershed scale forest structure from light detection and ranging (lidar) data (foliar biomass, stem density, basal area, and total biomass), and satellite-derived vegetation photosynthetic activity (enhanced vegetation index (EVI)). These data sets were compared with climatic and topographic metrics describing the spatial and temporal availability of water and energy. The overarching question of this study was: How does hillslope topography influence conifer growth, ecosystem biomass accumulation, and photosynthetic activity as watersheds transition from energy to water-limited conditions?

2. Materials and Methods

2.1. Study Area

The North Fork of Elk Creek (NFEC) (Figure 1) is a headwater catchment within the Lubrecht Experimental Forest, located in the Garnet Mountain Range in Western Montana. This 17.9 km^2 watershed has a 900 m elevation gradient with a mean elevation of 1,595 m. NFEC is drained by Elk Creek, a tributary of the Blackfoot river, a headwater of the Columbia River Basin. Regionally, NFEC is considered semiarid, where annual potential evapotranspiration exceeds actual evapotranspiration and annual precipitation is ~500 mm (Bailey, 1979). However, the deficit between potential evapotranspiration and actual transpiration (deficit = potential evapotranspiration-actual evapotranspiration) generally decreases both with increasing elevation and decreasing solar radiation (i.e., topoclimate effects).

Historical meteorological records of air temperature, precipitation, snow depth, and snow water equivalent are available from two snow survey telemetry (SNOTEL) stations located within NFEC (Lubrecht Flume station # 604, 1,426 m elevation, and N Fk Elk Creek station # 657, 1,905 m elevation). These stations have been recording since 1970 and 1967, respectively. Annually, the Lubrecht Flume SNOTEL site (low elevation) receives 514 mm of accumulated precipitation, while the N Fk Elk Creek SNOTEL site (high elevation) receives 664 mm (between 1981 and 2010). Water stored as snowpack accounts for 27% and 46% of annual precipitation for low and high elevations, respectively. The average annual temperature is 4.22°C and 2.98°C (calculated from years with continuous temperature data between 1981 and 2010) for low and high elevations, respectively. On average, lower elevations experience temperatures above 0°C 22 days earlier than higher elevations (day of year 68 and 90, respectively).

Three coniferous tree species, *Pseudotsuga menziesii* (Douglas fir, PSME), *Pinus ponderosa* (ponderosa pine, PIPO), and *Larix occidentalis* (western larch, LAOC) account for ~80% of stems in the Lubrecht Experimental Forest (PSME ~49.0%, PIPO ~17.6%, and LAOC ~12.8%) (Rowell et al., 2009). The other 20% of stems in the Lubrecht Experimental Forest are generally composed of *Pinus contorta* (lodepole pine), *Abies lasiocarpa* (subalpine fir), and *Picea engelmannii* (Engelmann spruce). The Anaconda Mining Company harvested timber at the forest from the period of 1904 to 1934, and as a result, the NFEC watershed was extensively clear-cut (Cauvin, 1961). This contributed to present-day stands of similar age that range from 70 to 100 years old. Historically (1700–1875), nonstand replacing fires burned in the Lubrecht Experimental forest once every 7 years and no major fires have occurred in Lubrecht Experimental Forest since 1871 (Grissino-Mayer et al., 2006). There is no documented history of insect outbreaks or disturbance prior to our study observation period.

The underlying lithology of the NFEC is predominantly composed of quartz monzonite. Surrounding the periphery of the watershed is a Mesoproterozoic metasedimentary unit known as the Belt Supergroup unit. This unit is comprised primarily of interbedded mudstones and fine-grained sandstones with occasional carbonate-muds (Winston & Link, 1993). Soils derived from these geologic formations are considered Typic Haplustalfs (National Cooperative Soil Survey, U.S. Department of Agriculture, 2001), a well-drained silty loam, with higher organic contents on northerly facing hillslopes. Soil depths are relatively consistent across sideslope (~0.5 m–1.0 m) and hollow (1.0 m–2.0 m) landscape positions based upon 54 soil water wells driven to bedrock and 54 soil pits.

2.1.1. Quantification of Ecosystem Productivity

We assessed three aspects of "ecosystem productivity" using ground measures of stemwood basal area increment and remotely sensed measures of biomass accumulation (forest structure) and forest greenness

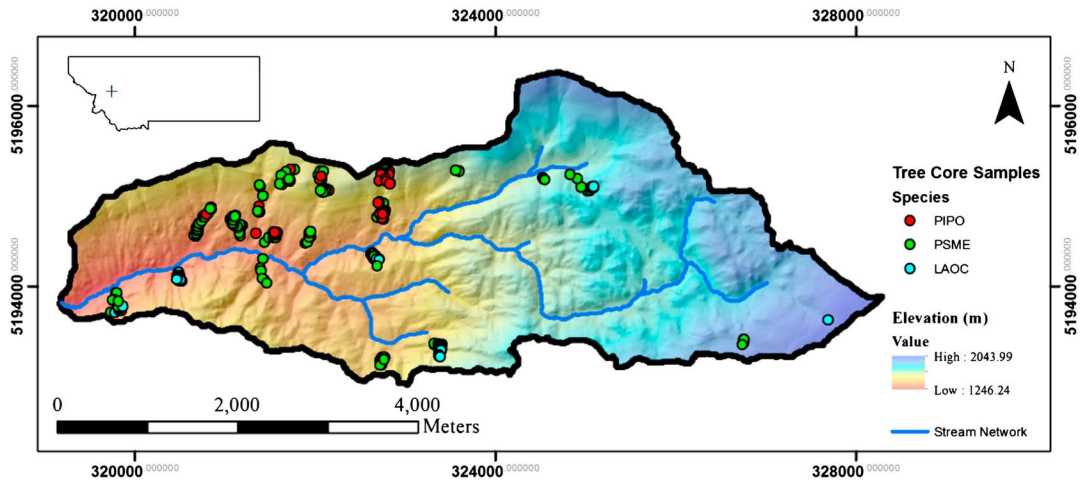

Figure 1. The location of the Lubrecht Experimental Forest within Montana and the North Fork of Elk Creek (NFEC) watershed located within the Lubrecht Experimental Forest. The colored circles represent the location of tree core samples, where the red, green, and blue represent ponderosa pine (PIPO), Douglas fir (PSME), and western larch (LAOC), respectively.

(photosynthetic activity). Ecosystem productivity has been measured, estimated, and defined in many ways. Direct observations of stem-specific productivity include basal area increment and diameter increment (West, 1980), changes in stem height (Skovsgaard & Vanclay, 2008), and measurements of biomass (Prescott et al., 1989), among others. Alternatively, direct measures of forest properties (i.e., stem height) can be applied to empirical relationships, producing modeled allometry of forest structure and productivity (Lefsky et al., 2005). Indirect measures of ecosystem productivity, such as observations of reflected light from vegetation (such as red and near-infrared light), are used to calculate measures of vegetation "greenness" (i.e., normalized difference vegetation index (NDVI) and enhanced vegetation index (EVI)). These metrics are useful because of their relation to the leaf area index and in turn, net primary productivity (Goward & Dye, 1987; Running et al., 2004). Combined, these measures represent different aspects of productivity that may be sensitive to different environmental factors and processes.

2.1.2. Stem Measures of Tree Productivity

We collected 308 tree core samples from NFEC across a range of landscape positions (hollows, sideslopes, and ridgelines), aspects, and elevations between 2013 and 2015 (Figure 1). This sampling regime was conducted to represent the larger watershed distribution of landscape positions and climatic settings. Trees from the three main species (PSME, PIPO, and LAOC) were randomly selected across hillslopes, and tree core samples were taken parallel to the local elevation contour lines. Spatial positioning of each stem was determined with a Trimble GeoXT Global Positioning System.

Increment cores were mounted, sanded, and scanned according to standard dendrochronological practices (Stokes & Smiley, 1968). Annual ring widths were measured using Cybis Dendrochronological Suite to the nearest 0.001 mm (Larsson, 2014). Visual cross-dating was conducted to identify missing rings, cracks, and to date individual tree cores (Stokes & Smiley, 1968). To quantify annual growth rates for each tree sampled, we calculated the annual basal area increment (BAI) for each ring:

$$\mathrm{BAI} = \pi r_i^2 - \pi r_{i-1}^2$$

where r_i is the radius of the tree at the end of annual ring production and r_{i-1} is the radius of the tree at the beginning of annual ring production. Cumulative growth curves were constructed for each stem by summing BAI for each year. Time for each cumulative growth curve was normalized between 0 (the first recorded ring) and 1 (the final recorded ring).

2.1.3. Lidar-Derived Estimates of Ecosystem Structure

Gridded data sets of stem density, basal area, foliar biomass, and total biomass were calculated by aggregating individual tree data derived from a stem detection algorithm applied to airborne light detection and ranging (lidar) point clouds collected in the Lubrecht Experimental Forest in 2005 (Rowell et al., 2009, Figure 2). We used basal area, stem density, total biomass, and foliar biomass as measures of forest structure and compared these data sets to metrics of hillslope topography and spatial climatic conditions.

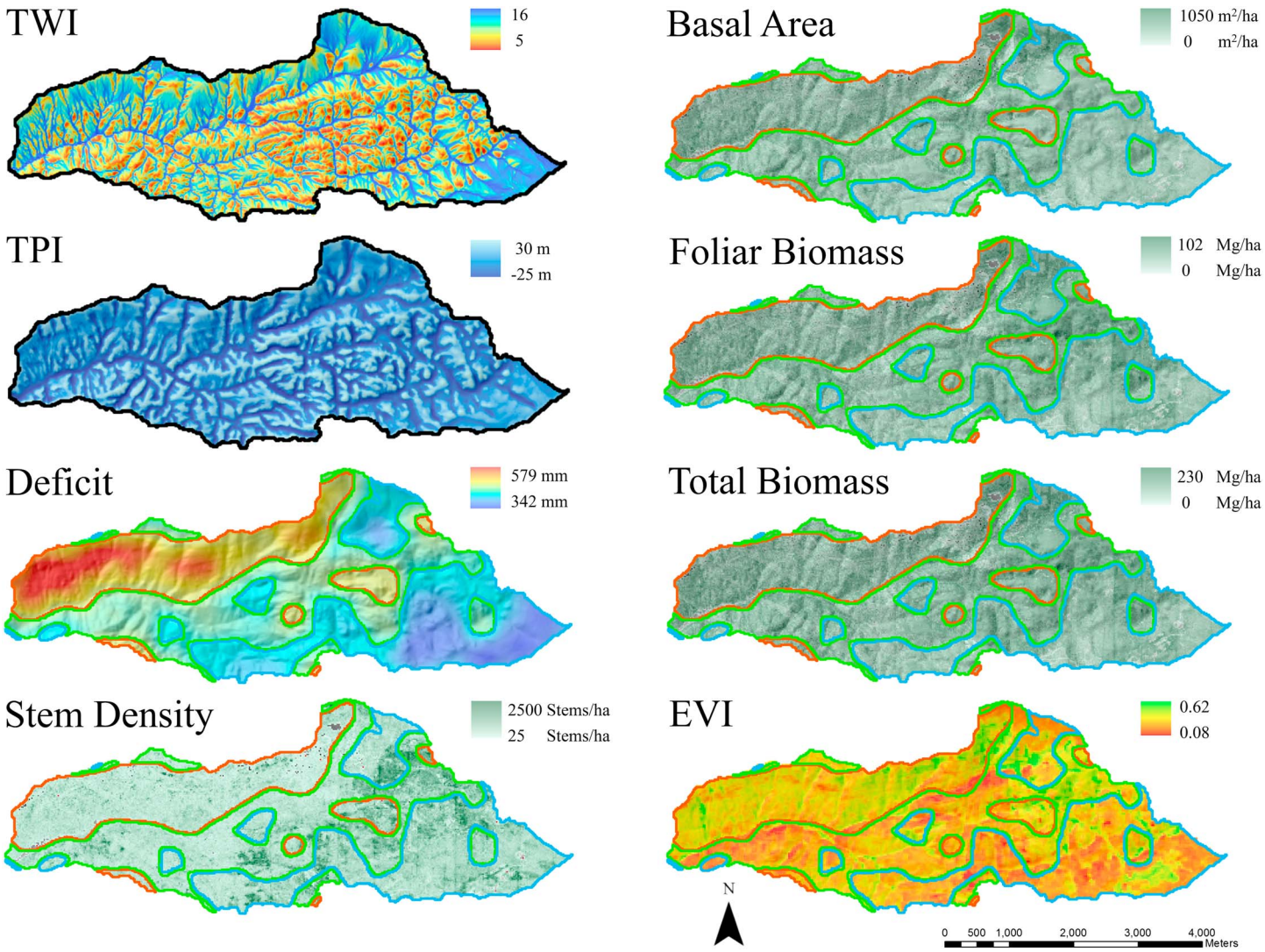

Figure 2. Maps representing topographic and climatic water balance data sets (topographic wetness index, TWI; topographic position index, TPI; climatic water deficit, deficit) and ecological response data sets (stem density, basal area, foliar biomass, total biomass, and average growing season enhanced vegetation index, EVI). The colored lines represent deficit class boundaries, where red is deficit > 460 mm, green is 460 mm > deficit > 423 mm, and blue is deficit < 423 mm.

The fundamental framework for selecting tree locations from lidar data was the utilization of a local maximum filter, which chooses the highest point in a neighborhood (i.e., the top of a tree), (Popescu et al., 2002) along with integration of structural parameters to inform expected crown width and hence, search radii of the local filter (Rowell et al., 2009, 2006). Following stem location, stem density was calculated by summing the number of stems in a 20 m × 20 m (400 m^2) neighborhood. Diameter at breast height was calculated for each stem using stem height, relative height (stem height normalized by mean stem height in neighborhood), and stem density for dominant and codominant stems. Basal area was subsequently calculated by aggregating stem diameter at breast height for the 20 m neighborhood. Foliar biomass and total biomass were then calculated using allometric models reported in Ter-Mikaelian and Korzukhin (1997) (all model parameters are reported in Rowell et al., 2009). Correlations between field measurements (61–400 m^2 plots, 1,555 individual trees) and laser-derived forest structural estimates were high (stem density: R^2 = 0.70, root-mean-square error (RMSE) = 17.36 stems; basal area: R^2 = 0.63, RMSE = 0.31 m^2; foliar biomass: R^2 = 0.78, RMSE = 100.2 kg; and total biomass: R^2 = 0.66, 714.8 kg) (Rowell et al., 2009). There were a total of 44,495 20 m pixels considered in the NFEC watershed for each lidar-derived product.

2.1.4. Watershed Greenness

We used forest greenness (the enhanced vegetation index (EVI)) as a general indicator of relative foliar photosynthetic activity (i.e., growing season activity). Metrics of vegetation greenness (EVI and NDVI) are commonly used as indicators of ecosystem photosynthesis and provide indirect measures of vegetation status and growth (Jensen & Lulla, 1987; Running & Nemani, 1988; Turner & Gardner, 2015; Wang et al., 2004). Greenness can also be used to evaluate relative magnitudes of and temporal variations in photosynthetic activity (Goetz et al., 1999; Myneni et al., 1995). EVI was developed to optimize detection of vegetation reflectance by reducing the influence of the canopy background signal and distortions in the atmosphere (Huete et al., 2002). EVI data sets were derived for NFEC from Landsat 5 spectral data using Google Earth Engine at a 30 m resolution (Figure 2). The Landsat 5 data were radiometrically calibrated and orthorectified using ground control points and digital elevation models to correct for relief displacement (Tucker et al., 2004). EVI was calculated as

$$\mathrm{EVI} = G \times \frac{(\mathrm{NIR} - \mathrm{RED})}{(\mathrm{NIR} + C1 \times \mathrm{RED} - C2 \times \mathrm{BLUE} + L)}$$

where NIR is the amount of near-infrared light, RED is the amount of red light reflected from the vegetation, BLUE is the amount of blue light reflected from the vegetation, and G, $C1$, $C2$, and L are constants (2.5, 6, 7.5, and 1, respectively). This algorithm is based on the physics of light absorption and scatter from chlorophyll (RED absorption) and mesophyll (NIR scatter) leaf structures (Myneni et al., 1995) during photosynthesis. The BLUE spectra corrects for distortions caused by aerosols in the atmosphere (Huete et al., 2002). A cloud removal algorithm was applied to each 16 day Landsat 5 image in order to remove any pixel that had a cloud likelihood score of 10% or higher from the analysis (Zhu et al., 2015). We removed all pixels within two vertical meters of the perennial stream network to remove effects of riparian vegetation (i.e., only forest environments were included in our analysis). We then calculated the median EVI of every pixel (from 1984 to 2012) for the growing season as a whole (1 June to 31 September), as well as each individual month. There were a total of 22,758 30 m pixels considered in the NFEC watershed for each EVI product.

2.2. Gridded Climate Data

Temperature and precipitation both affect forest carbon accumulation. However describing climate as a function of temperature and precipitation independently ignores their interplay that ultimately limits available water and energy in complex landscapes. Here we employed a simple climatic water balance approach (Stephenson, 1998) in order to describe water and energy limitations (topoclimate) and their potential impact on climate-forest interactions (Stephenson, 1998). Following methods described by Dobrowski et al. (2013), we developed gridded 250 m resolution soil water balance data from 1981 to 2010 at a monthly time step. Inputs to our model included daily temperature and solar radiation data described by Holden et al. (2016), monthly 800 m resolution PRISM precipitation data (Daly et al., 2008) and daily relative humidity and wind speed data from Abatzoglou (2013). We then aggregated these input data to a monthly time step and resampled to 250 m. Soil water holding capacity in the model was defined using gridded data provided by the Natural Resource Conservation Service Soil Survey Geographic Database retrieved at a resolution of 30 m and resampled to 250 m resolution. Outputs of the monthly model include potential evapotranspiration and actual evapotranspiration and the water balance deficit, representing the unmet atmospheric demand for moisture (potential evapotranspiration-actual evapotranspiration). We calculated the total annual deficit for each year and then calculated the average annual deficit from 1981 to 2010. The 30 year normal grid was then resampled to 20 and 30 m resolution to match the lidar and Landsat data sets, respectively. The product of this resampling technique was used to classify the watershed into tertiles of deficit to approximate climatically dry, moderate, and wet spatial regions (deficit $>$ 460 mm, 460 mm $>$ deficit $>$ 423 mm, deficit $<$ 423 mm, respectively; Figure 2).

2.3. Topographic Analysis:

We selected topographic indices to represent relevant spatial patterns of hydrologic and atmospheric conditions and describe potential water and energy availability at the hillslope scale. Topographic indices were computed using a 1 m^2 digital elevation model (DEM) derived from the lidar data set using the System for Automated Geoscientific Analyses geographic information system platform (Conrad et al., 2015). DEM pixel sizes were resampled to 10 m, 20 m, and 30 m resolution (100 m^2, 400 m^2, and 900 m^2 areas) to eliminate

Table 1
Table Representing the Multiple Linear Regression Model Selection Process

Variable	Coefficient	Adj R^2	P value	AIC	ΔAIC
Intercept	52.00	NA	NA	3531.88	NA
TWI	78.86	0.37	<0.01	3387.06	144.82
Species: Intercept interaction	2,279 (PIPO) 1,290 (LAOC)	0.47	<0.01	3341.76	45.30
Deficit	−0.5787	0.48	<0.01	3334.72	7.04
Species: Deficit interaction	−5.231 (PIPO) −3.287 (LAOC)	0.50	<0.01	3326.63	8.09
Species: TWI interaction	46.96 (PIPO) −4.542 (LAOC)	0.51	<0.01	3318.56	8.07
Basal area	NA	NA	NA	NA	NA
Stem density	NA	NA	NA	NA	NA
TPI	NA	NA	NA	NA	NA
Elevation	NA	NA	NA	NA	NA
Potential solar radiation	NA	NA	NA	NA	NA

Note. This model utilizes AIC to achieve the highest explanatory power while maintaining a parsimonious model. NA indicates not available.

microtopographic variations and to match ecological data set resolution for our correlation analysis. DEM-derived data sets included slope (β), upslope accumulated area (α), incoming annual potential solar radiation, the topographic position index, (TPI) and the topographic wetness index (TWI).

TWI is a hydrologic similarity index and has been used as a proxy for shallow soil moisture (Beven & Kirkby, 1979; Western et al., 1999) and lateral subsurface flow (Jencso et al., 2009). This metric accounts for nonlocal subsidies of water (upslope accumulated area) and local surface controls of water movement (local slope) (Figure 2). TWI is calculated as

$$\mathrm{TWI} = \ln\left(\frac{\alpha}{\tan(\beta)}\right)$$

where α is the upslope accumulated area of a given pixel and β is the local slope of a given pixel (Beven & Kirkby, 1979). The TWI has been spatially correlated to soil moisture; however, the strength of the correlation typically increases as antecedent moisture conditions increase toward gravity drainage (Western et al., 1999, 2004).

The TPI has been applied by researchers to classify hydrologic landforms and slope position classes (Tagil & Jenness, 2008; Weiss, 2001) and has been used to identify wet and dry landscape positions (De Reu et al., 2013). In this analysis we utilized the TPI to describe relative landscape positions with respect to a defined neighborhood (Figure 2). The algorithm used to derive TPI is

$$\mathrm{TPI} = \left(z_i - z_{f\mathrm{mean}(i)} + 0.5\right)$$

where z is the elevation for any given pixel (i) and $z_{f\mathrm{mean}}$ is the focal mean of pixel i at a given radius (Weiss, 2001). For this analysis focal radii were held constant at 150 m in order to preserve hillslope scale topographic convergence and divergence. Negative values of TPI are representative of convergent hillslope positions, and increasingly, positive TPI values transition from toe slopes to sideslopes to ridgelines (planar to divergent hillslope positions). Wet and dry landscapes are in convergent and divergent hillslope positions, respectively.

2.4. Assessment of Stemwood Productivity

We produced a multiple linear regression model using a multidirectional stepwise algorithm in order to assess the explanatory power of topographically derived predictor variables (R Core Team, 2015). This algorithm seeks to minimize the Akaike information criterion (AIC) value associated with each predictor variable permutation in order to produce the most parsimonious model (Venables & Ripley, 2002; Wagenmakers & Farrell, 2004). Variables included in the model, cumulative model fit (adjusted R^2), and P value (calculated from an analysis of variance) are reported in Table 1. Species designation was included as a factor variable to allow for species-specific interactions with predictor variables and modifications of model intercepts. The deficit was used to describe the spatial variability in the water balance and topoclimate at each stem's location across the watershed. Basal area and stem density were included to represent potential biotic interactions on growth, such as competition. The topographic metrics TWI, elevation, potential solar radiation, and TPI at each stem location were also included as potential predictor variables.

2.5. Assessment of Watershed Structure and Greenness

To assess watershed scale trends in forest structure and greenness, we first classified the watershed based on tertiles of deficit (deficit > 460 mm, 460 mm > deficit > 423 mm, deficit < 423 mm). This discretized the watershed into relatively water-limited, relatively moderate, and relatively energy-limited spatial regions, respectively, with even watershed areas in each class. We then classified the distribution of TPI within a deficit class into 100 quantile bins and extracted the median stem density, basal area, total biomass, foliar biomass, and EVI value for each TPI bin. In order to evaluate the degree of variance around each bin's median, we determined the interquartile range of each variable for each TPI bin. Subsequent nonlinear rational models were fit to the median values of each ecological variable across the TPI distribution to describe the behavior of each trend. We selected nonlinear rational models due to their ability to approximate linear trends, where

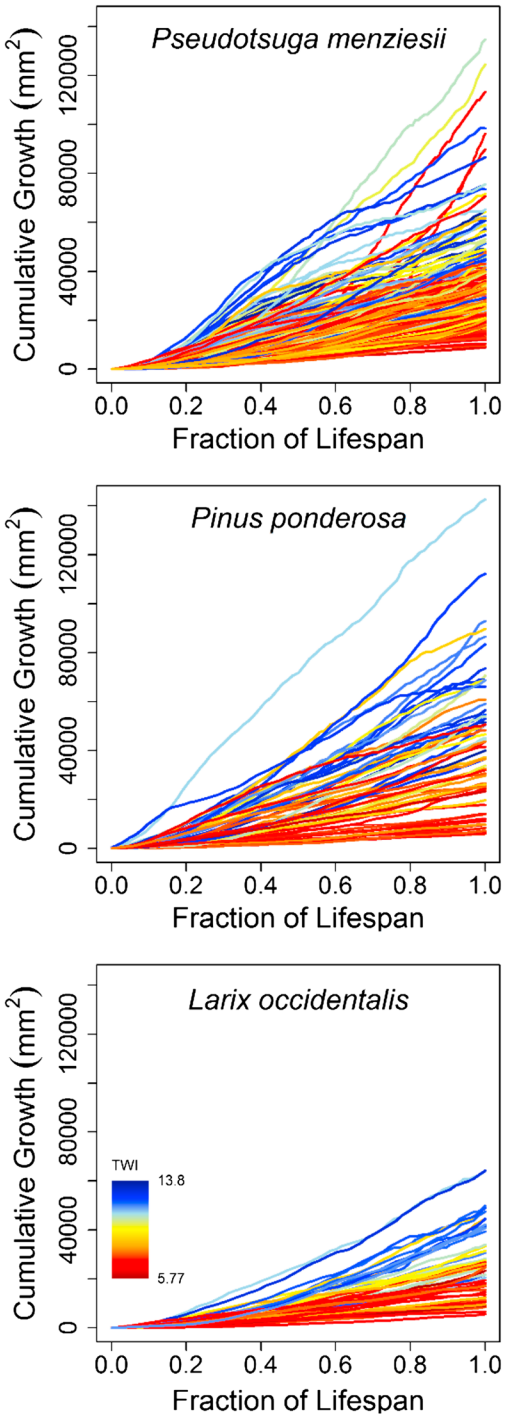

Figure 3. Cumulative basal area growth curves for each sampled tree stem by species. Each plot is normalized to the fraction of the trees total age and colored according to the TWI value at each sampled stem location. Generally, trees in wetter landscape positions (higher TWI) exhibited greater cumulative basal area growth across their life spans.

the rate of change of y given x is constant, and nonlinear trends, where the rate of change of y given x is nonlinear. Each regression is of the form

$$y = \frac{(a + bx)}{(1 + cx)}$$

where y is the response variable; a (intercept), b, and c (describe the shape of the nonlinear regression) are coefficients; and x (the median TPI value for the associated TPI quantile) is the predictor variable.

3. Results

3.1. Topographic, Climatic, and Physiological Effects on Ecosystem Productivity

Cumulative conifer growth was highly affected by topographic position (Figure 3), such that trees located in wet hillslope positions (Figure 3, blue lines) generally exhibited larger total growth than trees located in dry hillslope positions (Figure 3, red lines). This observation led us to quantify the effects of topographic position, species, and topoclimate on annual conifer growth rates. The multiple linear regression model (Table 1) used to describe variance in observed annual conifer growth rates (BAI) selected TWI as the primary predictor variable (adjusted R^2 = 0.37), followed by a species modification of the model intercept (adjusted R^2 = 0.47), the deficit (adjusted R^2 = 0.48), a species interaction with the deficit coefficient (adjusted R^2 = 0.50), and a species interaction with the TWI coefficient (combined adjusted R^2 = 0.51). In all cases TWI had a positive influence on annual growth rates. We did observe a species-specific response to the TWI, such that LAOC had the smallest growth rate response to TWI (74.31 mm^2 TWI^{-1}) followed by PSME (78.86 mm^2 TWI^{-1}) and PIPO (125.8 mm^2 TWI^{-1}). The deficit had a negative effect on BAI for all species, such that a higher climatic water deficit yielded lower annual growth rates. However, each species had a variable response to the deficit (PSME = −0.5787 mm^2 mm^{-1}, LAOC = −3.866 mm^2 mm^{-1}, and PIPO = −5.792 mm^2 mm^{-1}). All parameter selection and model fit statistics are reported in Table 1.

3.2. Topographic Effects on Forest Structure

At the watershed scale the TPI was chosen over the TWI to describe relative hillslope scale microclimatic conditions. Both TWI and TPI describe relative moisture conditions across landscapes (Western & Grayson, 1998; Weiss, 2001) but differ in terms of their assessment of terrain attributes. High TWI values (wet locations) are constrained to the most convergent locations in mountainous terrain due the metric sensitivity to upslope accumulated area and local slope. TPI represents a gradient in hillslope scale moisture conditions due to the difference in elevation between surrounding hillslope positions. The relationship between these metrics and a map showing the spatial variance between "wet" TWI and TPI hillslope positions are presented in the supporting information document S1.

Stem density decreased with increasing convergence in all cases; however, the relative sensitivity of each relationship was related to the deficit (Figures 4a–4c and Table 2). Stem density was relatively insensitive to TPI in locations of high deficit (Figure 4a and Table 2) and most sensitive to TPI in locations of moderate and low deficits (Figures 4b and 4c and Table 2), such that convergent hillslope positions had substantially less median stem density than divergent hillslope positions. The most negative TPI quantile (convergent) had 26%, 41%, and 41% lesser median stem density than the most positive TPI quantile (divergent) for each respective

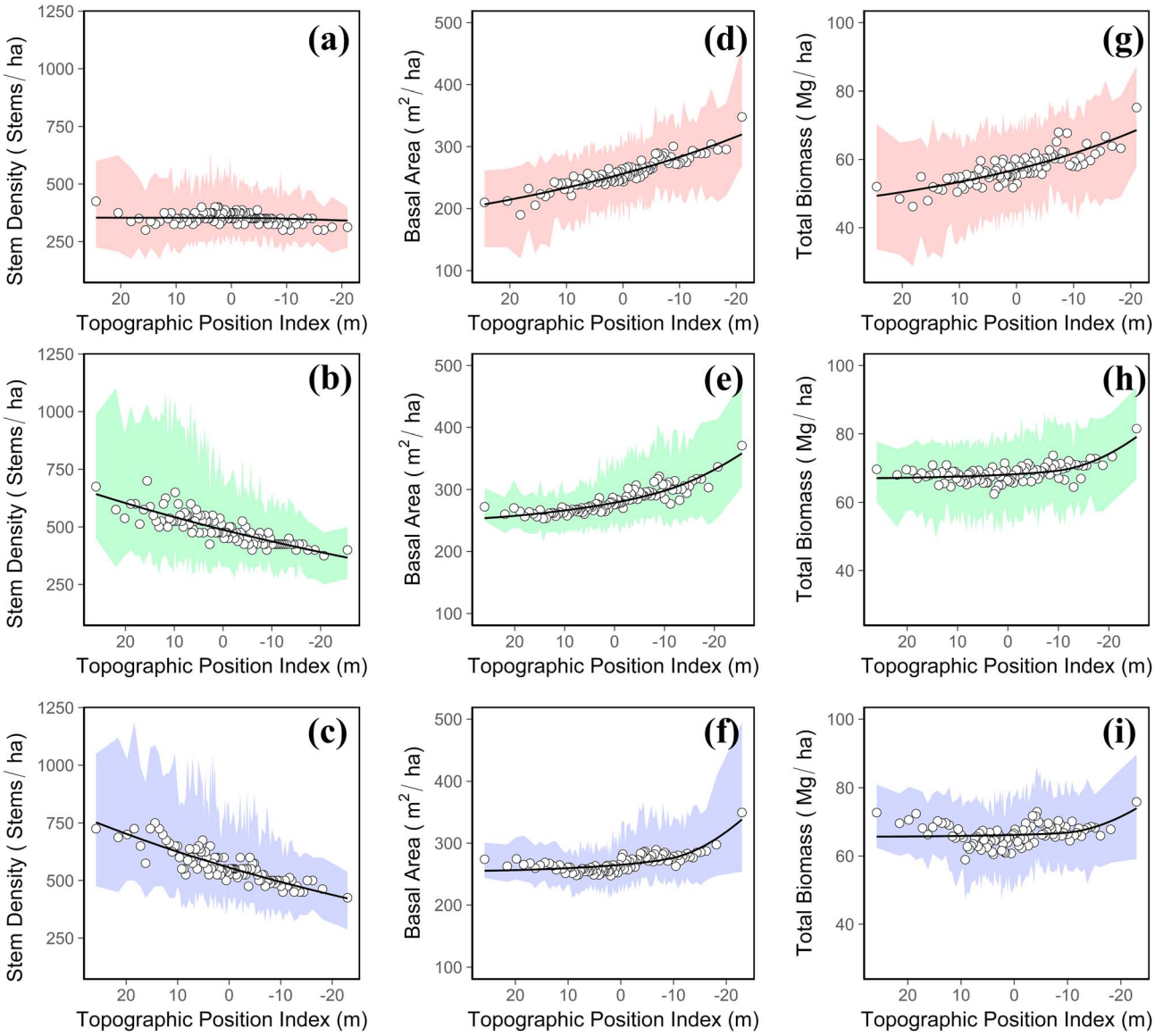

Figure 4. Scatterplots representing the median stem density, basal area, and total biomass within a given TPI class. Negative TPI values indicate wetter hillslope positions (i.e., hollows), and positive values are representative of drier hillslope positions (i.e., sideslopes to ridgelines). The black regression lines represent the nonlinear rational model used to describe the scatterplot shown. The colored ribbons about each point represent the interquartile range of the response variable's distribution within the associated TPI class. The color of each ribbon denotes the deficit class, where red is deficit > 460 mm, green is 460 mm > deficit > 423 mm, and blue is deficit < 423 mm.

deficit class (Table 2). The behavior of each model was relatively constant across all deficit classes, such that the nonlinear rational model approached a linear trend. Residual standard error (RSE) for each stem density model is 24.49, 36.01, and 36.75 stems/ha for high-, moderate-, and low-deficit classes, respectively (Table 2).

Basal area was differentially sensitive to hillslope position as a function of the deficit (Figures 4d–4f and Table 2). For all deficit classes, the most convergent hillslope positions exhibited greater median basal area than the most divergent hillslope positions. The most convergent TPI quantile had 66%, 36%, and 28% greater basal area than the most divergent TPI quantile for high-, moderate-, and low-deficit classes, respectively (Table 2). The rate of change of basal area with respect to TPI was relatively constant in locations of high deficit (Figure 4d and Table 2); however, basal area increased at a faster than linear rate in moderate- and low-deficit locations (Figures 4e and 4f and Table 2). RSE for each basal area model was 9.144, 9.016, and 8.364 m^2/ha for high-, moderate-, and low-deficit classes, respectively (Table 2).

Table 2
Table Summarizing Nonlinear Rational Model Fit, Parameters, and Selected Statistics Across Each Deficit Class and Response Variable

Deficit class/response variable	Model fit and parameters				Statistics			
	RSE	*a*	*b*	*c*	TPI	Median	Q1	Q3
Stem density (stems/ha)								
Deficit > 460 mm	24.49	352.7	18.78	0.053	−21.0	312.5	225.0	400.0
					24.5	425.0	225.0	600.0
460 mm > Deficit > 423 mm	36.01	487.7	3.158	−0.004	−25.5	400.0	275.0	500.0
					26.0	675.0	450.0	987.5
Deficit < 423 mm	36.75	556.2	3.563	−0.005	−23.0	425.0	287.5	537.5
					25.8	725.0	475.0	1050.0
Basal area (m^2/ha)								
Deficit > 460 mm	9.144	256.2	−0.186	0.009	−21.0	348.1	269.6	460.1
					24.5	209.7	137.7	261.2
460 mm > Deficit > 423 mm	9.016	278.7	4.362	0.021	−25.5	370.9	304.8	473.3
					26.0	272.0	249.2	301.9
Deficit < 423 mm	8.364	264.9	8.504	0.034	−23.0	349.4	253.9	494.6
					25.8	273.9	243.5	300.7
Foliar biomass (Mg/ha)								
Deficit > 460 mm	0.943	22.87	−0.062	0.003	−21.0	27.26	21.56	32.09
					24.5	21.70	14.08	29.78
460 mm > Deficit > 423 mm	0.868	27.83	−0.932	−0.033	−25.5	30.00	25.73	33.76
					26.0	29.45	24.81	33.06
Deficit < 423 mm	1.142	27.25	−0.901	−0.034	−23.0	28.60	23.23	33.29
					25.8	30.99	26.34	34.31
Total biomass (mg/ha)								
Deficit > 460 mm	2.570	57.07	0.281	0.012	−21.0	75.20	57.87	87.22
					24.5	52.01	33.64	70.41
460 mm > Deficit > 423 mm	1.959	68.12	2.203	0.033	−25.5	81.47	66.75	93.63
					26.0	69.65	60.19	77.73
Deficit < 423 mm	2.860	66.16	2.567	0.039	−23.0	75.84	59.11	89.62
					25.8	72.69	62.41	80.95

Convergent hillslope positions had larger amounts of median total biomass than divergent hillslope positions in locations of high and moderate deficits; however, there was little difference in locations of low deficit (Figures 4g–4i and Table 2). The most convergent TPI quantile had 45%, 17%, and 4% larger median total biomass than the most divergent TPI quantile for high-, moderate-, and low-deficit classes, respectively (Table 2). Similar to basal area, the rate of change of total biomass as a function of TPI was relatively constant in locations of high deficit (Figure 4g and Table 2); however, the rate of change became nonlinear in locations of moderate and low deficits (Figures 4h and 4i and Table 2). RSE for each total biomass model was 2.570, 1.959, and 2.860 Mg/ha for high-, moderate-, and low-deficit classes, respectively (Table 2).

Foliar biomass increased constantly with increasing hillslope convergence in locations of high deficit (Figure 5a and Table 2) showed little to no topographic dependence in locations of moderate deficit (Figure 5b and Table 2) and decreased with increasing convergence in locations of low deficit (Figure 5c and Table 2). The most convergent TPI quantile had 26% and 2% greater median foliar biomass than the most divergent quantile for high and moderate deficits and had 8% lesser median foliar biomass in locations of low deficit (Table 2). RSE for each foliar biomass model was 0.943, 0.868, and 1.142 Mg/ha for high-, moderate-, and low-deficit classes, respectively (Table 2).

3.3. Topographic Effects on Forest Greenness

In locations of high deficit, median growing season forest greenness increased consistently with increasing hillslope convergence (Figure 5d, scatter points and black trend line, and Table 3). However, relationships between hillslope convergence and greenness varied based on month (Figure 5d, colored trend lines, and Table 3). In the early growing season, monthly rates of change were similar to the median growing season behavior (June = blue line, July = green line; Table 3); however, greenness was generally higher across all values of TPI for these 2 months (Table 3). On average, June was the greenest month in locations of high deficit (Figure 5d, blue trendline, and Table 3). As the growing season progressed into August (Figure 5d,

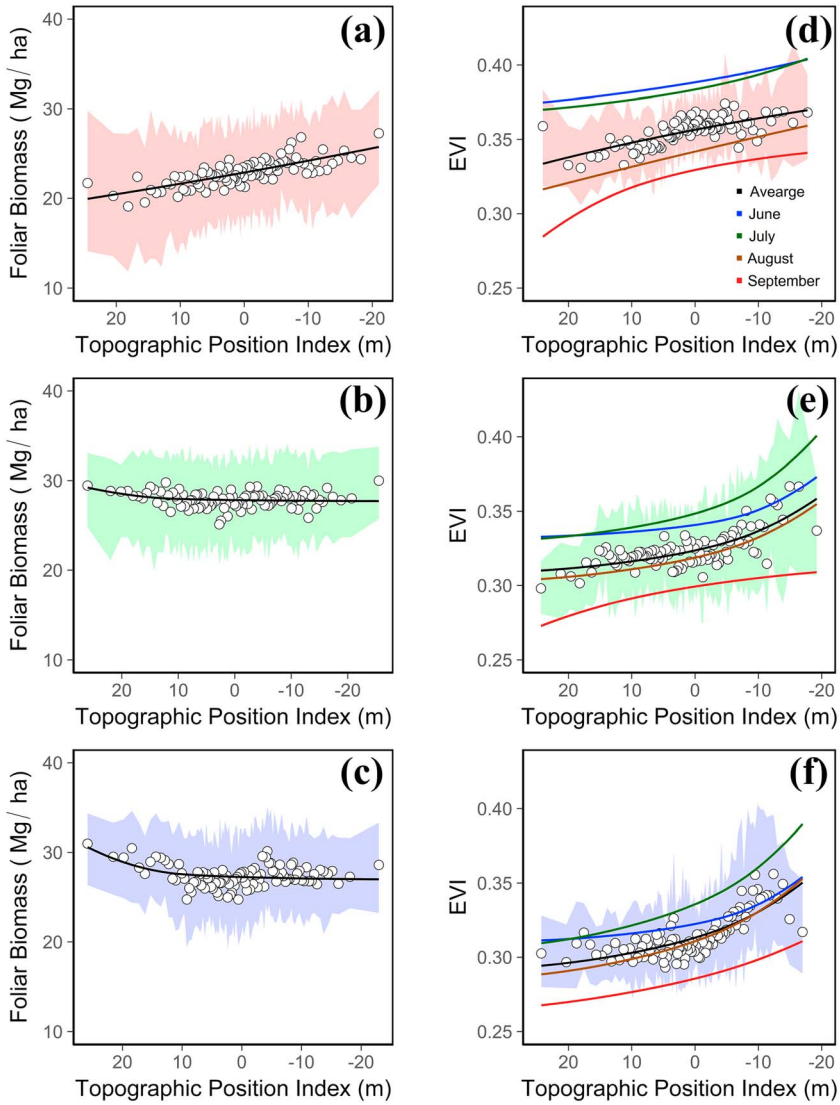

Figure 5. Scatterplots representing the median foliar biomass and EVI within a given TPI class. Negative TPI values indicate wetter hillslope positions (i.e., hollows), and positive values are representative of drier hillslope positions (i.e., sideslopes to ridgelines). The black regression lines represent the nonlinear rational model used to describe the scatterplot shown. The colored ribbons about each point represent the interquartile range of the response variable's distribution within the associated TPI class. The color of each ribbon denotes the deficit class, where red is deficit > 460 mm, green is 460 mm > deficit > 423 mm, and blue is deficit < 423 mm.

brown trendline) the average magnitude of greenness was reduced (Table 3); however, the rate of change with respect to hillslope convergence was similar to the growing season median (Table 3). In the late growing season (Figure 5d, red trendline) greenness was the lowest (Table 3) and increased nonlinearly from divergent to convergent hillslope positions (Table 3).

In locations of moderate deficit, median growing season greenness increased at a faster than linear rate from divergent to convergent hillslope positions (Figure 5e, scatter points and black trend line, and Table 3). The rate of change in June, July, and August were similar to the median growing season rate of change (Table 3). In September, greenness increased in a nonlinear fashion from divergent to convergent hillslope positions (Table 3). Generally, July exhibited the greenest values and September exhibited the least green values (Table 3).

In locations of low deficit (Figure 5f and Table 3), the growing season regression and each monthly regression exhibited a nonlinear increase in greenness with increasing landscape convergence (Table 3). Similar to moderate deficit locations, July was the greenest month and September was the least green month (Table 3).

Table 3
Table Summarizing Nonlinear Rational Model Fit and Parameters for Average Growing Season and Monthly EVI Across Each Deficit Class

	Model fit and parameters			
Deficit class/time	RSE	*a*	*b*	*c*
Growing season average				
Deficit > 460 mm	0.007	0.357	−0.003	−0.006
460 mm > Deficit > 423 mm	0.009	0.324	0.008	0.027
Deficit < 423 mm	0.009	0.313	0.007	0.026
June				
Deficit > 460 mm	0.008	0.388	0.003	0.010
460 mm > Deficit > 423 mm	0.007	0.341	0.011	0.035
Deficit < 423 mm	0.008	0.322	0.010	0.034
July				
Deficit > 460 mm	0.007	0.384	0.006	0.018
460 mm > Deficit > 423 mm	0.009	0.348	0.009	0.030
Deficit < 423 mm	0.011	0.336	0.007	0.027
August				
Deficit > 460 mm	0.006	0.342	−0.002	−0.002
460 mm > Deficit > 423 mm	0.009	0.319	0.007	0.026
Deficit < 423 mm	0.010	0.311	0.006	0.025
September				
Deficit > 460 mm	0.007	0.329	−0.008	−0.022
460 mm > Deficit > 423 mm	0.009	0.299	−0.006	−0.016
Deficit < 423 mm	0.009	0.286	0.004	0.017

4. Discussion

4.1. Hillslope Topography, Vegetation Physiology, and Climate Effects on Stem Productivity

Our results at both the stem and watershed scales suggest that hillslope topography is a highly influential factor for hillslope scale hydrometeorological conditions that lead to enhanced conifer productivity (Figure 3 and Table 1). The stem-based analysis of tree basal area increments indicated close to an order of magnitude difference in annual growth rates as stems transitioned from hollows with high TWIs to adjacent upslope areas with lower TWIs. In many instances these differences were associated with trees growing within 30 m of each other. This finding is striking and aligns with previous research, which suggests convergent hillslope positions with large upslope accumulated area and reduced slopes experience enhanced soil moisture (Beven & Kirkby, 1979; Western & Grayson, 1998; Western et al., 1999), a primary limiting resource for conifer growth in the western United States. Moreover, previous research has shown that divergent hillslope positions experience increased atmospheric demand, causing rapid moisture depletion due to exposure to wind (Chapman, 2000; Mikita & Klimánek, 2010) and solar radiation (Dubayah, 1994). Further, when moist antecedent soil conditions are coupled to landscape positions with sufficient upslope area, lateral subsurface flow can occur (Hwang et al., 2012; Jencso et al., 2009; Jencso & McGlynn, 2011), redistributing upslope hydrologic subsidies to biota in downslope positions. Thus, in semiarid watersheds, topographically induced microclimate and soil moisture availability in hillslope hollows can be decoupled from regional climate, likely ameliorating water limitations on conifer growth and modifying local ecosystem resilience to climate variability (Dobrowski, 2011; McLaughlin et al., 2017).

Another important factor selected to describe average conifer productivity was species designation (Table 1). In NFEC, species differences in minimum annual growth (model intercept), relative sensitivity to topoclimate (deficit-species interaction), and relative sensitivity to hillslope position (TWI-species interaction) were observed (Table 1). Physiological constraints on basal biomass accumulation via differences in water use efficiency (Zhang et al., 1996), vulnerability to drought-induced stress (Stout & Sala, 2003), and/or carbon allocation between roots, stems, and foliage (Poorter et al., 2012) likely account for variability in interspecies response to water availability across landscape positions. Another potential explanation for this effect is species-specific differences in wood density (Saranpää, 2003) causing variable average ring widths. Over time, these differences could create systematic differences in species-specific average BAI.

As we expected, spatial locations in the NFEC with increased deficit resulted in decreased annual growth rates for all species. However, deficit affected conifer growth rates to a lesser overall extent than local topography. For example, the ranges of linear model growth rates were 596.2 mm^2, 959.0 mm^2, and 530.2mm^2 across dry to wet TWI values but only ranged 103.0 mm^2, 399.6 mm^2, and 402.1 mm^2 across the deficit gradient for PSME, PIPO, and LAOC, respectively. To our knowledge, this is the first study to observe that local hydrometeorological conditions associated with hillslope topographic convergence and divergence can outweigh the impact of larger scale elevation and aspect effects on topoclimate and conifer growth rates in semiarid landscapes such as the NFEC.

Our study assessed the interplay between spatial variability in the climatic water balance, local topography, and stemwood growth rates. We did not assess conifer stemwood response to interannual climate variability. However, our findings generally concur with the conclusions of Bunn et al. (2005), Anning et al. (2013), and Adams et al. (2014), who observed differential conifer response to temperature and precipitation dynamics based on site moisture conditions. Bunn et al. (2005) found that *P. balfouriana* growing in divergent and high radiation settings were more sensitive to interannual patterns of precipitation than those in convergent, low radiation settings. Further, Anning et al. (2013) found that conifers in mesic sites had substantially less significant correlations with climatic variables than those in intermediate and xeric sites. Similarly, Adams et al. (2014) observed variability of conifer response to interannual precipitation and temperature regimes when

stems were positioned in low versus high TWI locations, suggesting that topography altered conifer growth response to climate. For example, *P. ponderosa* and *P. contorta* were less responsive to warm temperatures and *P. ponderosa* was less responsive to precipitation patterns when located in wet landscape positions. Collectively, these studies and our results suggest that landscape topography is an important consideration for both interannual growth and the spatial variability of conifers response to climate across larger watersheds.

4.2. Topographic Effects on Forest Structure

Convergent zones (i.e., –TPI values) accumulated larger amounts of total forest biomass across NFEC (Figures 4g–4i), reflecting observed differences in conifer growth rates (Table 1) and cumulative conifer growth (Figure 3) likely due to wetter hydrometeorological conditions (Martin et al., 2017). In general, basal area and total biomass increased as hillslope convergence increased; however, the relative sensitivity of basal area and total biomass to hillslope convergence varied by deficit (Figures 4d–4i). In locations of high deficit (i.e., low elevation, south aspect), where climatic constraints on water availability are large, topographically induced microclimate may be decoupled from regional climate in convergent hillslope positions. Therefore, gradients in topographic convergence and divergence in high deficit zones result in large spatial variations in forest structure and biomass accumulation that ranged from 52 to 75 Mg/ha (Figures 4d and 4g and Table 2). However, relationships between hillslope topography and basal area/total biomass became less linear as deficit decreased (Figures 4d–4i), possibly reflecting a reduced role of topographically induced microclimate for ecosystem productivity.

In locations of low deficit (Figures 4f and 4i; i.e., high elevation, northerly aspects), moisture distributions are likely more homogeneous between convergent and divergent hillslope positions due to increased precipitation and reductions in temperature at higher elevations (Figure 2). This reflects a tighter coupling between topographically induced microclimate and topoclimate. As a result, we observed less variance in basal area and total biomass across gradients in hillslope convergence and divergence. However, even in locations of low deficit, highly convergent hillslope positions may sustain moist conditions during the driest portion of the growing season and/or during long-term droughts (Figures 4f and 4i).

Our findings are consistent with recent work describing the topographic organization of mean carbon loading in conifer forests (Swetnam et al., 2017). Swetnam et al. (2017) observed the strongest topographic gradients of carbon loading in the driest basin evaluated (based on mean temperature and precipitation). However, we show that the topographic organization of forest structure varies substantially across intrabasin gradients in water availability, highlighting the importance of local gradients in the climatic water balance and suggesting that hydrologic refugia (McLaughlin et al., 2017) from topographic convergence may become increasingly important to terrestrial ecosystems as climate shifts toward increasing aridity (IPCC, 2014).

In the NFEC, convergent landscape positions were occupied by less dense forest stands with trees having larger basal areas and greater amounts of total biomass. This finding is consistent with results from the analysis of stemwood productivity in NFEC. For example, stem density was relatively homogeneous across hillslope positions in locations of high deficit (Figure 4a); however, stem density decreased with increasing hillslope convergence in locations of moderate and low deficits (Figures 4b and 4c), while basal area and total biomass generally increased with increasing hillslope convergence (Figures 4d–4i). Gradients in stem density across mountain landscapes are complex due to interactions between species specific phenology, seedling establishment, competition, and physical stresses encountered during growth (Berkowitz et al., 1995; Uhl et al., 2015). As a simplified explanation, these relationships could be an effect of interactions between gradients in abiotic stress (such as moisture availability) and competition (Callaway & Walker, 1997). Trees that are early to establish in convergent hillslope positions (where abiotic stress is low) likely out compete juveniles for light, limiting juvenile growth extensively, and therefore reducing local stem density. Alternatively, in divergent hillslope positions, increased water limitations may limit growth to a greater extent than competition, resulting in dense stands with reduced annual growth.

4.3. Topographic Effects on Forest Greenness

We attribute differences in vegetation greenness to gradients of photosynthetic activity, as opposed to differences in foliar biomass (Figures 5a–5c). Our results suggest that conifers in convergent zones are more photosynthetically active and experience extended growing seasons, likely due to differences in site

hydrometeorology. Furthermore, this suggests that across relatively acute to moderate climatic water limitations (from high to low deficits), hillslope convergence is a strong mediator of forest ecosystem photosynthesis throughout the growing season. Across all classes of deficit, average growing season greenness increased with increasing hillslope convergence (Figures 5d–5f, black trendlines). Temporal analysis (monthly regressions) indicated that convergent locations consistently hosted greener vegetation than divergent locations across time and space (Figures 5d–5f, colored trendlines). Other than in locations of high deficit, there was little spatial covariance between EVI and foliar biomass. This evidence corroborates both ground-based observations of spatial trends in forest productivity (Table 1) and remotely sensed forest biomass accumulation (Figures 4g–4i) along topographic gradients.

Similar to our results, greener vegetation has previously been observed along areas of convergence (Flores Cervantes et al., 2014), and along hydrologic flow paths (Hwang et al., 2012). Hwang et al. (2012) proposed that the degree of organization of vegetation along hydrologic flow paths effectively represents the dependency of local ecosystems to lateral redistribution of soil moisture. While we acknowledge that lateral redistribution of moisture likely plays a substantial role in organizing vegetation along topographic gradients, topographically organized transfers of water vapor and energy (i.e., vapor pressure gradients) also significantly impact spatial patterns of atmospheric demands for moisture and therefore, ecosystem productivity (Martin et al., 2017; Oberhuber et al., 2014). Furthermore, soil processes (such as weathering and transport) and properties (such as texture, depth, and composition) often align along topographic gradients (McAuliffe, 1994; Pachepsky et al., 2001; Rasmussen et al., 2011) and contribute to the organization of soil moisture and plant available nutrients. Future research should focus on understanding how both plant available water, atmospheric moisture conditions, and soil properties combine to influence growing season carbon accumulation across complex terrain.

Hillslope divergence becomes increasingly influential in dictating ecosystem greenness when acute climatic water limitations are exacerbated by hillslope form. For example, in September in locations of high and moderate deficit (Figures 5d and 5e, red trendlines), forest greenness declines rapidly with increasing hillslope divergence (from 0 to 20 TPI). This could reflect ecosystem response to extreme climatic aridity, subsequently intensified by divergent hillslope geometry, promoting a greater atmospheric demand for soil moisture (VPD) and downslope routing of soil water. Sufficiently high VPD and/or low soil moisture content could cause stomatal closure (Oren et al., 1999), therefore decreasing photosynthesis and greenness. Alternatively, divergent hillslope geometry (from 0 to 20 TPI) did not have a strong effect on vegetation greenness in relatively energy limited locations (low deficit; Figure 5f). This is likely because increased climatically driven moisture (due to orography) is available to conifers in divergent hillslope positions. Similar patterns of ecosystem response may provide further evidence of spatial regions where topographically induced microclimate is coupled or decoupled to regional climate (Dobrowski, 2011) at the global scale.

Under acute climatic water limitations (high deficit) the NFEC forest is the greenest in June (Figure 5d, blue trendline), which represents an early onset of maximum forest greenness. This is in contrast to moderate and low deficits (Figures 5e and 5f, green trendlines) where July is the greenest month. Generally, deficit decreases with increasing watershed elevation producing colder temperatures from low to high elevation. Temperature is a strong driver of many ecosystem processes including the onset of bud burst (Campbell & Sugano, 1975; Worrall, 1993) and early season photosynthesis (Tranquillini, 1964). This biophysical response would produce greener vegetation earlier in the growing season at lower elevations (generally in locations of high deficit). This is consistent with the observed 22 day average lag, where daily temperatures surpass 0°C, between high and low elevation SNOTEL sites at the NFEC. However, this lag between maximum forest greenness across deficit classes could also be due to differences in phenology between species. For instance, PIPO stands in NFEC tend to be located in low-elevation, high radiation environments (high deficit) and could respond differently to changes in photoperiod and temperature when compared to PSME or LAOC. Nonetheless, phenology and climate are intrinsically linked (Cleland et al., 2007), and thus, disentangling species versus climate signals from remotely sensed data is challenging without species distribution data sets.

5. Implications

In our semiarid watershed we attributed differences in spatial patterns of ecosystem productivity to the alignment of hillslope topography and topoclimate that caused differences in the persistence of

hydrometeorological processes such as vapor pressure deficit, shallow soil moisture distributions, and shallow subsurface flow. However, topography often emerges from feedback between different geomorphic processes under the influence of catchment properties such as surficial geology, soils, and vegetation. Each of these processes are dynamic in space and over climate timescales (centuries to millennia), leading to differential erosion rates within watersheds, and therefore spatial differences in soil textural distributions (McAuliffe, 1994). Convergent hillslope positions are typically depositional locations that can accumulate deep and finely textured soils that may therefore have increased water holding capacities (Pachepsky et al., 2001). In addition, nutrient availability has been shown to increase from upslope to downslope positions and with decreasing slope angle, generally tracking soil moisture content (Hilton et al., 2013; Tateno & Takeda, 2003; Weintraub et al., 2015).

In contrast to semiarid environments, mesic ecosystems have been shown to be progressively less productive as water availability becomes excessive relative to biological needs, due to reductions in local nutrient availability (Schuur & Matson, 2001). Mesic ecosystems also become increasingly productive with increasing site temperature (Schuur, 2003). We posit that a threshold is approached when regional climate limitations for forest growth transition from energy to water, at which point topographic convergence in complex terrain becomes a first-order control on landscape ecosystem productivity. This threshold exists because the dominating hydrometeorological and geomorphic processes, which impact ecosystems, vary spatially and temporally across watersheds globally, partially as a function of regional climate and the geometric form of a given watershed.

Our results suggest that two adjacent watersheds with the same climatic conditions may have vastly different ecosystem dynamics simply due to the degree of topographic complexity and the resultant hydrometeorological processes realized within the domain. This has global implications such that ecosystems nested within sufficiently complex terrain may have greater resilience to seasonal variations in moisture and temperature and longer term climate change. Increasing aridity across the western United States due to increasing temperature and changing precipitation distributions has ultimately led to decreased conifer forest productivity (Barnett et al., 2005; Churkina & Running, 1998; IPCC, 2014), increased susceptibility to mortality (McDowell et al., 2008; McDowell & Allen, 2015), and disturbances such as fire and pest infestations (Kaiser et al., 2013; Westerling et al., 2006). Consequently, topographically induced microclimates may become increasingly important for spatial patterns of ecosystem resilience and productivity as regional climate becomes more arid. The heterogeneity of landscapes across complex terrain will also impact future species distributions and migration routes of conifers into the future (Dobrowski & Parks, 2016).

6. Conclusion

Across one semiarid montane watershed we observed strong spatial and temporal variabilities in the organization of ecosystem productivity, structure, and photosynthetic activity due to hillslope topography and its location within a topoclimatic continuum. These findings suggest the need to consider both regional-topoclimate and its topology with hillslope positions of contrasting topographic complexity. As spatial climatic water limitations became more intense across an orographic gradient, patterns of ecosystem productivity were highly related to topographic convergence and divergence. Our findings suggest that in arid and semiarid environments, local hillslope convergence may provide zones of hydrologic refugia to biota by reducing atmospheric demand for soil moisture and enhancing shallow soil moisture availability (Dobrowski, 2011; McLaughlin et al., 2017). Thus, hydrometeorological processes operating across complex terrain in water limited climates have the potential to buffer biota from climate fluctuations by mediating edaphic and atmospheric moisture conditions (Adams et al., 2014; Anning et al., 2013; Bunn et al., 2005). Alternatively, as climatic moisture limitations decreased (i.e., northerly aspects at high elevation), patterns of ecosystem biomass were less related to topographic convergence and divergence. In this case, limitations of ecosystem productivity may be more impacted by alternative processes, such as local energy availability, soil and nutrient composition, or biotic competition. Future research should focus on understanding the interplay of hydrologic, soil, and nutrient processes that lead to gradients in ecosystem productivity across topography and climate gradients. Proper mechanistic descriptions of these localized processes, their persistence and sensitivity to future climate changes, are imperative for quantifying ecosystem productivity and zones of climate refugium at regional scales.

Acknowledgments
This work was made possible by a USDA NIFA McIntire Stennis award 233327 to Jencso and NSF grants DEB-1457749 and DEB-1457720 to Jencso and Hu. Additional support was provided by NSF EPSCoR through the Montana Institute on Ecosystems. The authors appreciate extensive logistic support from the staff of the Lubrecht Experimental Forest, especially Forest Manager, Frank Maus. All data used for the analyses presented in this manuscript are available in Data Set S1. We would like to thank the anonymous reviewers for their thoughtful comments and suggestions, which improved this manuscript.

References

Abatzoglou, J. T. (2013). Development of gridded surface meteorological data for ecological applications and modelling. *International Journal of Climatology*, *33*(1), 121–131. https://doi.org/10.1002/joc.3413

Adams, H. R., Barnard, H. R., & Loomis, A. K. (2014). Topography alters tree growth–climate relationships in a semi-arid forested catchment. *Ecosphere*, *5*(11), 1–16.

Allen, C. D., Macalady, A. K., Chenchouni, H., Bachelet, D., McDowell, N., Vennetier, M., … Gonzalez, P. (2010). A global overview of drought and heat-induced tree mortality reveals emerging climate change risks for forests. *Forest Ecology and Management*, *259*(4), 660–684. https://doi.org/10.1016/j.foreco.2009.09.001

Anning, A. K., Rubino, D. L., Sutherland, E. K., & McCarthy, B. C. (2013). Dendrochronological analysis of white oak growth patterns across a topographic moisture gradient in southern Ohio. *Dendrochronologia*, *31*(2), 120–128. https://doi.org/10.1016/j.dendro.2012.10.002

Bailey, H. P. (1979). Semi-arid climates: Their definition and distribution. In *Agriculture in semi-arid environments* (pp. 73–97). Berlin, Heidelberg: Springer. https://doi.org/10.1007/978-3-642-67328-3_3

Barnard, D. M., Barnard, H. R., & Molotch, N. P. (2017). Topoclimate effects on growing season length and montane conifer growth in complex terrain. *Environmental Research Letters*, *12*(6), 064003. https://doi.org/10.1088/1748-9326/aa6da8

Barnett, T. P., Adam, J. C., & Lettenmaier, D. P. (2005). Potential impacts of a warming climate on water availability in snow-dominated regions. *Nature*, *438*(7066), 303–309. https://doi.org/10.1038/nature04141

Berkowitz, A. R., Canham, C. D., & Kelly, V. R. (1995). Competition vs. facilitation of tree seedling growth and survival in early successional communities. *Ecology*, *76*(4), 1156–1168. https://doi.org/10.2307/1940923

Beven, K. J., & Kirkby, M. J. (1979). A physically based, variable contributing area model of basin hydrology/Un modèle à base physique de zone d'appel variable de l'hydrologie du bassin versant. *Hydrological Sciences Journal*, *24*(1), 43–69. https://doi.org/10.1080/02626667909491834

Biederman, J. A., Scott, R. L., Goulden, M. L., Vargas, R., Litvak, M. E., Kolb, T. E., … Burns, S. P. (2016). Terrestrial carbon balance in a drier world: The effects of water availability in southwestern North America. *Global Change Biology*, *22*(5), 1867–1879. https://doi.org/10.1111/gcb.13222

Bonan, G. (2015). *Ecological Climatology: Concepts and Applications*. Cambridge: Cambridge University Press.

Bunn, A. G., Waggoner, L. A., & Graumlich, L. J. (2005). Topographic mediation of growth in high elevation foxtail pine (Pinus balfouriana Grev. et Balf.) forests in the Sierra Nevada, USA. *Global Ecology and Biogeography*, *14*(2), 103–114. https://doi.org/10.1111/j.1466-822X.2005.00141.x

Callaway, R. M., & Walker, L. R. (1997). Competition and facilitation: A synthetic approach to interactions in plant communities. *Ecology*, *78*(7), 1958–1965. https://doi.org/10.1890/0012-9658(1997)078%5B1958:CAFASA%5D2.0.CO;2

Campbell, R. K., & Sugano, A. I. (1975). Phenology of bud burst in Douglas-fir related to provenance, photoperiod, chilling, and flushing temperature. *Botanical Gazette*, *136*(3), 290–298. https://doi.org/10.1086/336817

Cauvin, D. M. (1961). *Management plan for Lubrecht forest*. Missoula, MT: University of Montana Scholarworks.

Cervantes, F., Javier, H., Istanbulluoglu, E., Vivoni, E. R., Holifield Collins, C. D., & Bras, R. L. (2014). A geomorphic perspective on terrain-modulated organization of vegetation productivity: Analysis in two semiarid grassland ecosystems in southwestern United States. *Ecohydrology*, *7*(2), 242–257. https://doi.org/10.1002/eco.1333

Chapman, L. (2000). Assessing topographic exposure. *Meteorological Applications*, *7*(4), 335–340. https://doi.org/10.1017/S1350482700001729

Chen, J., Saunders, S. C., Crow, T. R., Naiman, R. J., Brosofske, K. D., Mroz, G. D., … Franklin, J. F. (1999). Microclimate in forest ecosystem and landscape ecology: Variations in local climate can be used to monitor and compare the effects of different management regimes. *Bioscience*, *49*(4), 288–297. https://doi.org/10.2307/1313612

Churkina, G., & Running, S. W. (1998). Contrasting climatic controls on the estimated productivity of global terrestrial biomes. *Ecosystems*, *1*(2), 206–215. https://doi.org/10.1007/s100219900016

Cleland, E. E., Chuine, I., Menzel, A., Mooney, H. A., & Schwartz, M. D. (2007). Shifting plant phenology in response to global change. *Trends in Ecology & Evolution*, *22*(7), 357–365. https://doi.org/10.1016/j.tree.2007.04.003

Conrad, O., Bechtel, B., Bock, M., Dietrich, H., Fischer, E., Gerlitz, L., … Böhner, J. (2015). System for Automated Geoscientific Analyses (SAGA) v. 2.1.4. *Geoscientific Model Development*, *8*(7), 1991–2007. https://doi.org/10.5194/gmd-8-1991-2015

Daly, C., Halbleib, M., Smith, J. I., Gibson, W. P., Doggett, M. K., Taylor, G. H., … Pasteris, P. P. (2008). Physiographically sensitive mapping of climatological temperature and precipitation across the conterminous United States. *International Journal of Climatology*, *28*(15), 2031–2064. https://doi.org/10.1002/joc.1688

De Reu, J., Bourgeois, J., Bats, M., Zwertvaegher, A., Gelorini, V., De Smedt, P., … Van Meirvenne, M. (2013). Application of the topographic position index to heterogeneous landscapes. *Geomorphology*, *186*, 39–49. https://doi.org/10.1016/j.geomorph.2012.12.015

Dobrowski, S. Z. (2011). A climatic basis for microrefugia: The influence of terrain on climate. *Global Change Biology*, *17*(2), 1022–1035. https://doi.org/10.1111/j.1365-2486.2010.02263.x

Dobrowski, S. Z., Abatzoglou, J., Swanson, A. K., Greenberg, J. A., Mynsberge, A. R., Holden, Z. A., & Schwartz, M. K. (2013). The climate velocity of the contiguous United States during the 20th century. *Global Change Biology*, *19*(1), 241–251. https://doi.org/10.1111/gcb.12026

Dobrowski, S. Z., & Parks, S. A. (2016). Climate change velocity underestimates climate change exposure in mountainous regions. *Nature Communications*, *7*, 12349. https://doi.org/10.1038/ncomms12349

Dubayah, R. C. (1994). Modeling a solar radiation topoclimatology for the Rio Grande River basin. *Journal of Vegetation Science*, *5*(5), 627–640. https://doi.org/10.2307/3235879

Emanuel, R. E., Riveros-Iregui, D. A., McGlynn, B. L., & Epstein, H. E. (2011). On the spatial heterogeneity of net ecosystem productivity in complex landscapes. *Ecosphere*, *2*(7), 1–13.

Fekedulegn, D., Hicks, R. R., & Colbert, J. J. (2003). Influence of topographic aspect, precipitation and drought on radial growth of four major tree species in an Appalachian watershed. *Forest Ecology and Management*, *177*(1-3), 409–425. https://doi.org/10.1016/S0378-1127(02)00446-2

Franks, P. J., Drake, P. L., & Froend, R. H. (2007). Anisohydric but isohydrodynamic: Seasonally constant plant water potential gradient explained by a stomatal control mechanism incorporating variable plant hydraulic conductance. *Plant, Cell & Environment*, *30*(1), 19–30. https://doi.org/10.1111/j.1365-3040.2006.01600.x

Fu, P., & Rich, P. M. (2002). A geometric solar radiation model with applications in agriculture and forestry. *Computers and Electronics in Agriculture*, *37*(1-3), 25–35. https://doi.org/10.1016/S0168-1699(02)00115-1

Gholz, H. L. (1982). Environmental limits on aboveground net primary production, leaf area, and biomass in vegetation zones of the Pacific Northwest. *Ecology*, *63*(2), 469–481. https://doi.org/10.2307/1938964

Goetz, S. J., Prince, S. D., Goward, S. N., Thawley, M. M., & Small, J. (1999). Satellite remote sensing of primary production: An improved production efficiency modeling approach. *Ecological Modelling*, *122*(3), 239–255. https://doi.org/10.1016/S0304-3800(99)00140-4

Goward, S. N., & Dye, D. G. (1987). Evaluating North American net primary productivity with satellite observations. *Advances in Space Research*, *7*(11), 165–174. https://doi.org/10.1016/0273-1177(87)90308-5

Grimm, N. B., Groffman, P., Staudinger, M., & Tallis, H. (2016). Climate change impacts on ecosystems and ecosystem services in the United States: Process and prospects for sustained assessment. *Climatic Change*, *135*(1), 97–109. https://doi.org/10.1007/s10584-015-1547-3

Grissino-Mayer, H. D., Gentry, C. M., Croy, S., Hiatt, J., Osborne, B., Stan, A., & Wight, G. D. (2006). Fire history of western Montana forested landscapes via tree-ring analyses. *Professional Paper*, *23*, 47–56.

Hänninen, H., & Tanino, K. (2011). Tree seasonality in a warming climate. *Trends in Plant Science*, *16*(8), 412–416. https://doi.org/10.1016/j.tplants.2011.05.001

Hilton, R. G., Galy, A., West, A. J., Hovius, N., & Roberts, G. G. (2013). Geomorphic control on the δ^{15}N of mountain forests. *Biogeosciences*, *10*(3), 1693–1705. https://doi.org/10.5194/bg-10-1693-2013

Hock, R., & Holmgren, B. (2005). A distributed surface energy-balance model for complex topography and its application to Storglaciären, Sweden. *Journal of Glaciology*, *51*(172), 25–36. https://doi.org/10.3189/172756505781829566

Holden, Z. A., Swanson, A., Klene, A. E., Abatzoglou, J. T., Dobrowski, S. Z., Cushman, S. A., … Oyler, J. W. (2016). Development of high-resolution (250 m) historical daily gridded air temperature data using reanalysis and distributed sensor networks for the US Northern Rocky Mountains. *International Journal of Climatology*, *36*(10), 3620–3632. https://doi.org/10.1002/joc.4580

Huete, A., Didan, K., Miura, T., Rodriguez, E. P., Gao, X., & Ferreira, L. G. (2002). Overview of the radiometric and biophysical performance of the MODIS vegetation indices. *Remote Sensing of Environment*, *83*(1-2), 195–213. https://doi.org/10.1016/S0034-4257(02)00096-2

Hwang, T., Band, L. E., Vose, J. M., & Tague, C. (2012). Ecosystem processes at the watershed scale: Hydrologic vegetation gradient as an indicator for lateral hydrologic connectivity of headwater catchments. *Water Resources Research*, *48*, W06514. https://doi.org/10.1029/2011WR011301

IPCC (2014). In Core Writing Team, R. K. Pachauri, & L. A. Meyer (Eds.), *Climate change 2014: Synthesis report. Contribution of working groups I, II and III to the fifth assessment report of the intergovernmental panel on climate change* (151 pp.). Geneva, Switzerland.

Jencso, K. G., & McGlynn, B. L. (2011). Hierarchical controls on runoff generation: Topographically driven hydrologic connectivity, geology, and vegetation. *Water Resources Research*, *47*, W11527. https://doi.org/10.1029/2011WR010666

Jencso, K. G., McGlynn, B. L., Gooseff, M. N., Wondzell, S. M., Bencala, K. E., & Marshall, L. A. (2009). Hydrologic connectivity between landscapes and streams: Transferring reach-and plot-scale understanding to the catchment scale. *Water Resources Research*, *45*, W0442. https://doi.org/10.1029/2008WR007225

Jensen, J. R., & Lulla, K. (1987). *Introductory digital image processing: A remote sensing perspective*. Englewood Cliffs, NJ: Taylor & Francis.

Kaiser, K. E., McGlynn, B. L., & Emanuel, R. E. (2013). Ecohydrology of an outbreak: Mountain pine beetle impacts trees in drier landscape positions first. *Ecohydrology*, *6*(3), 444–454. https://doi.org/10.1002/eco.1286

Körner, C. (2006). Significance of temperature in plant life. In *Plant growth and climate change* (pp. 48–69). Oxford, UK: Blackwell. https://doi.org/10.1002/9780470988695.ch3

Kramer, P. J., & Boyer, J. S. (1995). *Water relations of plants and soils*. San Diego, CA: Academic Press.

Larsson, L. (2014). CooRecorder and Cdendro programs of the CooRecorder/Cdendro package version 7.7.

Lefsky, M. A., Turner, D. P., Guzy, M., & Cohen, W. B. (2005). Combining lidar estimates of aboveground biomass and Landsat estimates of stand age for spatially extensive validation of modeled forest productivity. *Remote Sensing of Environment*, *95*(4), 549–558. https://doi.org/10.1016/j.rse.2004.12.022

Martin, J., Looker, N., Hoylman, Z., Jencso, K., & Hu, J. (2017). Hydrometeorology organizes intra-annual patterns of tree growth across time, space and species in a montane watershed. *New Phytologist*, *215*(4), 1387–1398. https://doi.org/10.1111/nph.14668

McAuliffe, J. R. (1994). Landscape evolution, soil formation, and ecological patterns and processes in Sonoran Desert bajadas. *Ecological Monographs*, *64*(2), 111–148. https://doi.org/10.2307/2937038

McDowell, N. G., & Allen, C. D. (2015). Darcy's law predicts widespread forest mortality under climate warming. *Nature Climate Change*, *5*(7), 669–672. https://doi.org/10.1038/nclimate2641

McDowell, N., Pockman, W. T., Allen, C. D., Breshears, D. D., Cobb, N., Kolb, T., … Yepez, E. A. (2008). Mechanisms of plant survival and mortality during drought: Why do some plants survive while others succumb to drought? *New Phytologist*, *178*(4), 719–739. https://doi.org/10.1111/j.1469-8137.2008.02436.x

McLaughlin, B. C., Ackerly, D. D., Klos, P. Z., Natali, J., Dawson, T. E., & Thompson, S. E. (2017). Hydrologic refugia, plants, and climate change. *Global Change Biology*, *23*(8), 2941–2961. https://doi.org/10.1111/gcb.13629

Mikita, T., & Klimánek, M. (2010). Topographic exposure and its practical applications. *Journal of Landscape Ecology*, *3*(1), 42–51.

Myneni, R. B., Dong, J., Tucker, C. J., Kaufmann, R. K., Kauppi, P. E., Liski, J., … Hughes, M. K. (2001). A large carbon sink in the woody biomass of northern forests. *Proceedings of the National Academy of Sciences of the United States of America*, *98*(26), 14,784–14,789. https://doi.org/10.1073/pnas.261555198

Myneni, R. B., Hall, F. G., Sellers, P. J., & Marshak, A. L. (1995). The interpretation of spectral vegetation indexes. *IEEE Transactions on Geoscience and Remote Sensing*, *33*(2), 481–486. https://doi.org/10.1109/36.377948

Novick, K. A., Oishi, A. C., & Miniat, C. F. (2016). Cold air drainage flows subsidize montane valley ecosystem productivity. *Global Change Biology*, *22*(12), 4014–4027. https://doi.org/10.1111/gcb.13320

Oberhuber, W., Gruber, A., Kofler, W., & Swidrak, I. (2014). Radial stem growth in response to microclimate and soil moisture in a drought-prone mixed coniferous forest at an inner Alpine site. *European Journal of Forest Research*, *133*(3), 467–479. https://doi.org/10.1007/s10342-013-0777-z

Oberhuber, W., & Kofler, W. (2000). Topographic influences on radial growth of Scots pine (Pinus sylvestris L.) at small spatial scales. *Plant Ecology*, *146*(2), 229–238. https://doi.org/10.1023/A:1009827628125

Oren, R., Sperry, J. S., Katul, G. G., Pataki, D. E., Ewers, B. E., Phillips, N., & Schäfer, K. V. R. (1999). Survey and synthesis of intra-and interspecific variation in stomatal sensitivity to vapour pressure deficit. *Plant, Cell & Environment*, *22*(12), 1515–1526. https://doi.org/10.1046/j.1365-3040.1999.00513.x

Pachepsky, Y. A., Timlin, D. J., & Rawls, W. J. (2001). Soil water retention as related to topographic variables. *Soil Science Society of America Journal*, *65*(6), 1787–1795. https://doi.org/10.2136/sssaj2001.1787

Pan, Y., Birdsey, R. A., Fang, J., Houghton, R., Kauppi, P. E., Kurz, W. A., … Ciais, P. (2011). A large and persistent carbon sink in the world's forests. *Science*, *333*(6045), 988–993. https://doi.org/10.1126/science.1201609

Poorter, H., Niklas, K. J., Reich, P. B., Oleksyn, J., Poot, P., & Mommer, L. (2012). Biomass allocation to leaves, stems and roots: Meta-analyses of interspecific variation and environmental control. *New Phytologist*, *193*(1), 30–50. https://doi.org/10.1111/j.1469-8137.2011.03952.x

Popescu, S. C., Wynne, R. H., & Nelson, R. F. (2002). Estimating plot-level tree heights with lidar: Local filtering with a canopy-height based variable window size. *Computers and Electronics in Agriculture*, *37*(1-3), 71–95. https://doi.org/10.1016/S0168-1699(02)00121-7

Prescott, C. E., Corbin, J. P., & Parkinson, D. (1989). Biomass, productivity, and nutrient-use efficiency of aboveground vegetation in four Rocky Mountain coniferous forests. *Canadian Journal of Forest Research*, *19*(3), 309–317. https://doi.org/10.1139/x89-046

Rasmussen, C. (2012). Thermodynamic constraints on effective energy and mass transfer and catchment function. *Hydrology and Earth System Sciences*, *16*(3), 725–739. https://doi.org/10.5194/hess-16-725-2012

Rasmussen, C., Troch, P. A., Chorover, J., Brooks, P., Pelletier, J., & Huxman, T. E. (2011). An open system framework for integrating critical zone structure and function. *Biogeochemistry*, *102*(1-3), 15–29. https://doi.org/10.1007/s10533-010-9476-8

Richardson, A. D., Keenan, T. F., Migliavacca, M., Ryu, Y., Sonnentag, O., & Toomey, M. (2013). Climate change, phenology, and phenological control of vegetation feedbacks to the climate system. *Agricultural and Forest Meteorology*, *169*, 156–173. https://doi.org/10.1016/j.agrformet.2012.09.012

Rosenzweig, M. L. (1968). Net primary productivity of terrestrial communities: Prediction from climatological data. *The American Naturalist*, *102*(923), 67–74. https://doi.org/10.1086/282523

Rossi, S., Deslauriers, A., Griçar, J., Seo, J. W., Rathgeber, C. B., Anfodillo, T., … Jalkanen, R. (2008). Critical temperatures for xylogenesis in conifers of cold climates. *Global Ecology and Biogeography*, *17*(6), 696–707. https://doi.org/10.1111/j.1466-8238.2008.00417.x

Rossi, S., Morin, H., Deslauriers, A., & Plourde, P. Y. (2011). Predicting xylem phenology in black spruce under climate warming. *Global Change Biology*, *17*(1), 614–625. https://doi.org/10.1111/j.1365-2486.2010.02191.x

Rowell, E., Seielstad, C., Goodburn, J., & Queen, L. (2009). Estimating plot-scale biomass in a western North American mixed-conifer forest from lidar-derived tree stems. In *Proceedings SilviLaser conference* (pp. 14–16). College Station, TX: Proceedings SilviLaser Conference.

Rowell, E., Seielstad, C., Vierling, L., Queen, L., & Shepperd, W. (2006). Using laser altimetry-based segmentation to refine automated tree identification in managed forests of the Black Hills, South Dakota. *Photogrammetric Engineering & Remote Sensing*, *72*(12), 1379–1388. https://doi.org/10.14358/PERS.72.12.1379

Running, S. W. (1984). Microclimate control of forest productivity: Analysis by computer simulation of annual photosynthesis/transpiration balance in different environments. *Agricultural and Forest Meteorology*, *32*(3-4), 267–288. https://doi.org/10.1016/0168-1923(84)90054-6

Running, S. W., & Nemani, R. R. (1988). Relating seasonal patterns of the AVHRR vegetation index to simulated photosynthesis and transpiration of forests in different climates. *Remote Sensing of Environment*, *24*(2), 347–367. https://doi.org/10.1016/0034-4257(88)90034-X

Running, S. W., Nemani, R. R., Heinsch, F. A., Zhao, M., Reeves, M., & Hashimoto, H. (2004). A continuous satellite-derived measure of global terrestrial primary production. *AIBS Bulletin*, *54*(6), 547–560.

Saranpää, P. (2003). Wood density and growth. In *Wood quality and its biological basis* (pp. 87–117). Oxford, UK: Blackwell.

Schuur, E. A. (2003). Productivity and global climate revisited: The sensitivity of tropical forest growth to precipitation. *Ecology*, *84*(5), 1165–1170. https://doi.org/10.1890/0012-9658(2003)084%5B1165:PAGCRT%5D2.0.CO;2

Schuur, E. A., & Matson, P. A. (2001). Net primary productivity and nutrient cycling across a mesic to wet precipitation gradient in Hawaiian montane forest. *Oecologia*, *128*(3), 431–442. https://doi.org/10.1007/s004420100671

Skovsgaard, J. P., & Vanclay, J. K. (2008). Forest site productivity: A review of the evolution of dendrometric concepts for even-aged stands. *Forestry: An International Journal of Forest Research*, *81*(1), 13–31. https://doi.org/10.1093/forestry/cpm041

Stephenson, N. (1998). Actual evapotranspiration and deficit: Biologically meaningful correlates of vegetation distribution across spatial scales. *Journal of Biogeography*, *25*(5), 855–870. https://doi.org/10.1046/j.1365-2699.1998.00233.x

Stokes, M. A., & Smiley, T. L. (1968). *An introduction to tree–ring dating*. Chicago: University of Chicago Press.

Stout, D. L., & Sala, A. (2003). Xylem vulnerability to cavitation in *Pseudotsuga menziesii* and *Pinus ponderosa* from contrasting habitats. *Tree Physiology*, *23*(1), 43–50. https://doi.org/10.1093/treephys/23.1.43

Swetnam, T. L., Brooks, P. D., Barnard, H. R., Harpold, A. A., & Gallo, E. L. (2017). Topographically driven differences in energy and water constrain climatic control on forest carbon sequestration. *Ecosphere*, *8*(4), e01797. https://doi.org/10.1002/ecs2.1797

Tagil, S., & Jenness, J. (2008). GIS-based automated landform classification and topographic, landcover and geologic attributes of landforms around the Yazoren Polje, Turkey. *Journal of Applied Sciences*, *8*(6), 910–921. https://doi.org/10.3923/jas.2008.910.921

Tague, C., & Dugger, A. L. (2010). Ecohydrology and climate change in the mountains of the western USA—A review of research and opportunities. *Geography Compass*, *4*(11), 1648–1663. https://doi.org/10.1111/j.1749-8198.2010.00400.x

Tateno, R., & Takeda, H. (2003). Forest structure and tree species distribution in relation to topography-mediated heterogeneity of soil nitrogen and light at the forest floor. *Ecological Research*, *18*(5), 559–571. https://doi.org/10.1046/j.1440-1703.2003.00578.x

Team, R. C. (2015). A language and environment for statistical computing. Vienna, Austria. 2014. Foundation for Statistical Computing; 2014.

Ter-Mikaelian, M. T., & Korzukhin, M. D. (1997). Biomass equations for sixty-five North American tree species. *Forest Ecology and Management*, *97*(1), 1–24. https://doi.org/10.1016/S0378-1127(97)00019-4

Tovar-Pescador, J., Pozo-Vázquez, D., Ruiz-Arias, J. A., Batlles, J., López, G., & Bosch, J. L. (2006). On the use of the digital elevation model to estimate the solar radiation in areas of complex topography. *Meteorological Applications*, *13*(03), 279–287. https://doi.org/10.1017/S1350482706002258

Tranquillini, W. (1964). The physiology of plants at high altitudes. *Annual Review of Plant Physiology*, *15*(1), 345–362. https://doi.org/10.1146/annurev.pp.15.060164.002021

Tucker, C. J., Grant, D. M., & Dykstra, J. D. (2004). NASA's global orthorectified Landsat data set. *Photogrammetric Engineering & Remote Sensing*, *70*(3), 313–322. https://doi.org/10.14358/PERS.70.3.313

Turner, M. G., & Gardner, R. H. (2015). Ecosystem processes in heterogeneous landscapes. In *Landscape ecology in theory and practice* (pp. 287–332). New York: Springer.

Uhl, E., Biber, P., Ulbricht, M., Heym, M., Horváth, T., Lakatos, F., … Pretzsch, H. (2015). Analysing the effect of stand density and site conditions on structure and growth of oak species using Nelder trials along an environmental gradient: Experimental design, evaluation methods, and results. *Forest Ecosystems*, *2*(1), 1–19.

U.S. Department of Agriculture, National Cooperative Soil Survey. (2001). Official Soil Series Descriptions: Lubrecht Series (Revision No. NRS-CNG-JAL). Retrieved from https://soilseries.sc.egov.usda.gov/OSD_Docs/L/LUBRECHT.html

Vapaavuori, E. M., Rikala, R., & Ryyppö, A. (1992). Effects of root temperature on growth and photosynthesis in conifer seedlings during shoot elongation. *Tree Physiology*, *10*(3), 217–230. https://doi.org/10.1093/treephys/10.3.217

Venables, W. N., & Ripley, B. D. (2002). *Modern applied statistics with S* (4th ed). New York: Springer.

Wagenmakers, E. J., & Farrell, S. (2004). AIC model selection using Akaike weights. *Psychonomic Bulletin & Review*, *11*(1), 192–196. https://doi.org/10.3758/BF03206482

Wang, J., Rich, P. M., Price, K. P., & Kettle, W. D. (2004). Relations between NDVI and tree productivity in the central Great Plains. *International Journal of Remote Sensing*, *25*(16), 3127–3138. https://doi.org/10.1080/0143116032000160499

Weintraub, S. R., Taylor, P. G., Porder, S., Cleveland, C. C., Asner, G. P., & Townsend, A. R. (2015). Topographic controls on soil nitrogen availability in a lowland tropical forest. *Ecology*, *96*(6), 1561–1574. https://doi.org/10.1890/14-0834.1

Weiss, A. (2001). Topographic position and landforms analysis. Poster presentation, ESRI user conference (Vol. 200). San Diego, CA.

West, P. W. (1980). Use of diameter increment and basal area increment in tree growth studies. *Canadian Journal of Forest Research*, *10*(1), 71–77. https://doi.org/10.1139/x80-012

Westerling, A. L., Hidalgo, H. G., Cayan, D. R., & Swetnam, T. W. (2006). Warming and earlier spring increase western US forest wildfire activity. *Science*, *313*(5789), 940–943. https://doi.org/10.1126/science.1128834

Western, A. W., & Grayson, R. B. (1998). The Tarrawarra data set: Soil moisture patterns, soil characteristics, and hydrological flux measurements. *Water Resources Research*, *34*(10), 2765–2768. https://doi.org/10.1029/98WR01833

Western, A. W., Grayson, R. B., Blöschl, G., Willgoose, G. R., & McMahon, T. A. (1999). Observed spatial organization of soil moisture and its relation to terrain indices. *Water Resources Research*, *35*(3), 797–810. https://doi.org/10.1029/1998WR900065

Western, A. W., Zhou, S. L., Grayson, R. B., McMahon, T. A., Blöschl, G., & Wilson, D. J. (2004). Spatial correlation of soil moisture in small catchments and its relationship to dominant spatial hydrological processes. *Journal of Hydrology*, *286*(1-4), 113–134. https://doi.org/10.1016/j.jhydrol.2003.09.014

Whittaker, R. H., & Niering, W. A. (1975). Vegetation of the Santa Catalina Mountains, Arizona. V. Biomass, production, and diversity along the elevation gradient. *Ecology*, *56*(4), 771–790. https://doi.org/10.2307/1936291

Winston, D., & Link, P. K. (1993). Middle Proterozoic rocks of Montana, Idaho and eastern Washington: The Belt Supergroup. In J. C. Reed Jr., et al. (Eds.), *Precambrian: Conterminous US Geological Society of America, The Geology of North America C-2* (pp. 487–517). Boulder, CO: Geological Society of America.

Winstral, A., & Marks, D. (2002). Simulating wind fields and snow redistribution using terrain-based parameters to model snow accumulation and melt over a semi-arid mountain catchment. *Hydrological Processes*, *16*(18), 3585–3603. https://doi.org/10.1002/hyp.1238

Worrall, J. (1993). Temperature effects on bud-burst and leaf-fall in subalpine larch. *Journal of Sustainable Forestry*, *1*(2), 1–18. https://doi.org/10.1300/J091v01n02_01

Zhang, J., Marshall, J. D., & Fins, L. (1996). Correlated population differences in dry matter accumulation, allocation, and water-use efficiency in three sympatric conifer species. *Forest Science*, *42*(2), 242–249.

Zhu, Z., Wang, S., & Woodcock, C. E. (2015). Improvement and expansion of the Fmask algorithm: Cloud, cloud shadow, and snow detection for Landsats 4–7, 8, and Sentinel 2 images. *Remote Sensing of Environment*, *159*, 269–277. https://doi.org/10.1016/j.rse.2014.12.014